Lateral buckling of drillstrings revisited: localised "snaking"

Ciprian D. Coman[1†]

[1] *Department of Computer Science, School of Computing & Engineering, University of Huddersfield, HD1 3DH, Huddersfield, UK*

March 12, 2023

Abstract

The classical lateral buckling of a straight drillstring confined within an inclined cylindrical borehole is formulated as a singularly-perturbed boundary-value problem which is subsequently explored by using asymptotic techniques. In particular, the localised nature of the critical eigenmodes is discussed with the help of a special multiple-scale technique that yields simple and accurate approximations for the corresponding critical loads. The asymptotic formulae obtained capture the dependence of these loads on the magnitude of the frictional forces as well as the inclination angle of the confining borehole.

Keywords: drillstrings, eigenvalue problems, localised deformations, asymptotic methods.

[†] cdc3p@yahoo.com

1 Introduction

Most traditional mechanical structures are designed to withstand buckling deformations, which are often seen as undesirable and act as a potential source of compromising their load-carrying capacity. This is not always possible in the case of highly flexible configurations such as the drillstrings used in accessing natural hydrocarbon reservoirs; the variability of the axial loads to which these structures are routinely exposed during normal drilling operations increases their susceptibility to the adverse effects of buckling. Indeed, it can be argued that *elastic* buckling of tubulars (drillstring or casing) is almost unavoidable during drilling and completion operations (e.g., see [1, 2, 3]). It is therefore not surprising that interest in the stability analysis of downhole tubulars has invariably played a key part in drilling design (e.g., see [4, 5, 6] and the references therein). Both the qualitative and quantitative understanding of the buckling of these structures are important to prevent costly failures and develop efficient future technologies for drilling highly deviated, horizontal, and extended reach wells that could unlock further access to currently unreachable energy resources.

Although there are many similarities between buckling of a drillstring (DS for short) and the traditional beam-column elastic stability theory [7, 8, 9], some key differences exist as well. For example, in vertical wells the weight of the DS might be solely responsible for the compressive forces exerted on its lower part; this introduces variable coefficients in the corresponding buckling equations [10, 11]. In fact, a typical DS is usually characterised by the presence of a *neutral point* that marks the boundary between two idealised non-overalapping one-dimensional regions which are either in tension or in compression. Another significant difference is that, unlike the classical buckling scenarios discussed in standard textbooks, the buckling of a DS takes place within the confined space of a cylindrical borehole. Such geometrical constraints can lead to exotic buckled shapes in the post-buckling regime, the most common being a spiral-like configuration [5, 6]. As it will be explained shortly, in deviated straight wells it is also necessary to consider situations in which the DS lies on the low side of the cylindrical boreholes; the typical buckling modes in this case are of the "snaking" type like the ones illustrated in Figure 1. The *localised* shape seen on the right in Figure 1 is the most

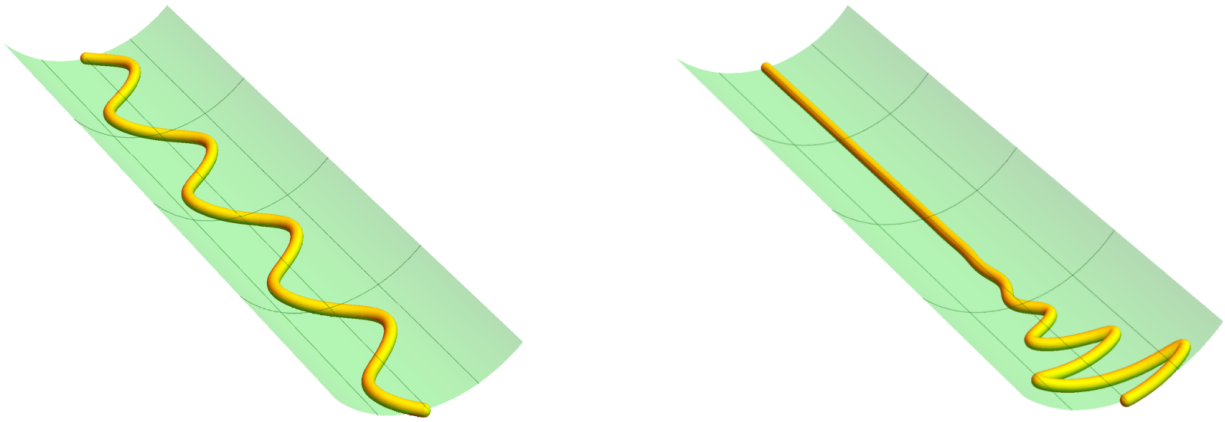

Figure 1: Typical "snaking" buckling patterns in an inclined borehole: *periodic* (left) and *localised* (right). Before buckling takes place the DS is assumed to lie on the low side of the borehole wall (shown as the green concave surface).

prevalent one, with the other one (on the left) being typically encountered in horizontal wells (when frictional effects are disregarded).

The starting point for the systematic exploration of elastic buckling phenomena in the context of oil and gas drilling operations is often linked to Lubinski's classical paper [12]. Apparently, this represents the first attempt of its kind in which mathematical/mechanical modelling was employed to deal specifically with the buckling of long DSs laterally constrained within a vertical cylindrical borehole. The analysis was limited to a two-dimensional setting and was based on a third-order ordinary differential equation with a linear coefficient. Power series solutions were used to formulate the corresponding determinantal equation whose solutions were then found numerically. Some further insight into the implications of buckling for drilling operations was provided in a couple of follow-up works [13, 14], which included the effects of DS internal pressure and buoyancy forces. Lubinksi's papers are conveniently collected in book form [15], where one can also find various discussions and critiques stimulated by the original publication of those papers.

Almost a decade before the publication of [12], Willers [16] studied an identical equation in connection with the buckling of a heavy vertical rod; his paper complements an even earlier study by Greenhill [17] and provides a more rational mathematical analysis than [12], being based on either Bessel or Lommel functions together with their asymptotic approximations. Some of the quantitative results reported in [16] were much later found to be inaccurate because an insufficient number of terms was retained in the corresponding approximations (e.g., see [18]). Rothman [19] re-discovered Willers' equation in his study involving axially symmetric deformations of an infinite elastic strip subjected to compressive edge loads acting at a constant angle to the plane of the plate. Suitable re-scaling of the physical quantities involved allowed him to obtain a general compact solution based on the Airy functions and their integrals (e.g., see [20]). Dunayevsky and Judzis [21] extended Lubinski's original work [12] by including the effect of an applied torque and allowing for three-dimensional deformations of a heavy vertical DS without any borehole constraints (see [22, 23] as well). The two coupled equations for the lateral displacements of their DS were written as a third-order complex-valued single differential equation having a very similar form to that studied previously in [16, 19]. This facilitated a closed-form solution in terms of the Airy functions and their integrals (as in Rothman's work) that eventually allowed those authors to obtain a simplified asymptotic relation connecting the applied critical compression and torque to other geometrical and mechanical parameters in their problem.

Three-dimensional buckling in the presence of an additional end-torque of a DS placed inside an inclined borehole was first explored by Paslay and Bogy [24]. While the applied compressive forces remained below the buckling threshold, their originally straight DS was taken to lie along the low side of a rigid circular cylinder. Once buckling was trigerred the deformed shape of this configuration was still assumed to remain in full contact with the inner surface of the cylinder, but frictional forces were disregarded. The relevant bifurcation equation was derived variationally by considering a suitable expression for the potential energy of the DS (including the effect of lifting around the borehole wall), with the help of nonlinear elasticity kinematics [25]. As the applied torque was discovered to be a secondary effect it was eventually neglected, and so was the relative rotation of the transverse cross-sections. These simplifications made it possible to obtain a relatively simple fourth-order differential equation with variable (linear) coefficients. Its solution was routinely computed by taking advantage of the simply-supported boundary conditions and using a finite Fourier sine series approximation. For a non-horizontal borehole the critical eigenmode turns out to be localised, as already seen in the right sketch of Figure 1; in the horizontal case the buckling equation reduces to that of a beam on a linear elastic foundation [26, 27], with its corresponding solution being a regular sinusoid similar to that in the left sketch of the same Figure. In a complementary study, Bogy and Paslay [28] examined the (planar) buckling of a heavy DS in the vertical axial plane of an inclined borehole; that is, the lateral displacements of the DS were restricted to be perpendicular to an inclined plane. In principle, the results of their second study can be used in conjunction with the earlier one ([24]) in order to predict

which type of buckling is energetically more favourable.

Broadly speaking, the motivation for the present study is partly related to the recent monograph [29], in which Gulyayev *et al.* have collected in one place a broad spectrum of topics related to drillstring mechanics. This is a welcome addition to the literature, not least because the authors follow an applied mathematics approach and do not rely excessively on purely numerical solutions. Another notable features include the systematic introduction of frictional forces in many of the mechanical models proposed, as well as the careful formulation of the corresponding boundary-value problems studied. Although reference [29] emphasises the singularly-perturbed character of many of the situtions encountered in drillstring mechanics, no serious attempts were made to capitalise on this observation. It is the purpose of this paper to discuss in some detail the asymptotic behaviour of one of the buckling models included in Chapter 7 of [29]. This model is an extension of that proposed earlier by Paslay and Bogy [24], in the sense that it incorporates (albeit in a simplified form) the neglected frictional effect of the contact interaction between the DS and the inner surface of the borehole.

A large portion of the extensive literature on static elastic instabilities in the oil well drilling is concerned with the so-called *helical buckling*. Such "buckling" is the result of secondary bifurcations that occur in the post-buckling regime but this fact is hardly acknowledged in the literature (the word "buckling" is a bit of a misnomer in this context). Work on this form of instability started with another paper by Lubinski *et al.* [30], who proposed a simplified semi-inverse approach to determine an approximate relationship between the terminal loads on the DS and the pitch of an infinitely long regular helix (representing the deformed DS). Subsequent efforts concentrated on refining the original model [30] by including the effect of boundary conditions, the spatial non-uniformity of the helical configuration, frictional forces, and so on. As this vast body of work is only tangentially relevant to our immediate goals, we refer the interested readers to the surveys [3, 4, 5, 6], which contain numerous pointers to the literature.

With this background in mind, we begin our study in §2 with a quick review of the linearised bifurcation problem for a heavy DS in an *inclined straight borehole*, and in the presence of simple dry friction. By casting the relevant fourth-order differential equation in non-dimensional form it proves possible to identify the sizes of the various coefficients in that equation as a function of an intuitive asymptotic parameter. A summary of several key direct numerical simulations of this non-dimensional bifurcation problem is included in §3. We also take this opportunity to rectify some of the innaccurate statements made in [29]; in particular, we show that the critical eigenmodes are localised near either the right or the left ends of the DS, depending on the value of the borehole inclination angle relative to a critical value (which is defined in the next section). The information gleaned from these numerical results is later exploited in §4 to flesh out the asymptotic structure of the eigenvalue problem that governs the buckling of the DS. As it happens, this asymptotic structure turns out to be quite different from that already investigated previously in similar contexts (e.g., [18, 19, 21]) and requires a major change of tack. We note in passing that the behaviour of the critical eigenmodes in the present study shares several salient features in common with our previous work [31, 32, 33, 34, 35] dealing with the wrinkling of various thin plate or shell configurations. The paper concludes in §5 with a brief discussion of the main results and their extensions to related situations.

2 Formulation

A succinct account of the key differential equations and assumptions used in the rest of the paper is presented in this section. The mathematical model we are planning to explore was discussed at length in references [29] (pp. 407-437) or [36], to which interested readers are referred for full details and

derivations. Here, we will be content in just highlighting those aspects that are required in order to make the paper reasonably self-contained.

During normal drilling of an oil well the DS is periodically pulled out of the borehole in order to replace a worn cutting element (the so-called 'drill bit') or a damaged drill pipe segment. Once this has been completed, the DS is lowered back into the borehole, by ensuring that the right amount of thrust is supplied to the lower end of the DS so that drilling can resume as efficiently as possible. For example, too much thrust can result in buckling of the DS, while too little can cause poor drilling efficiency by decreasing the rate of penetration [1, 2]. It is this type of scenario that the above-mentioned model targets.

To be more specific, the situation of interest concerns an inclined straight cylindrical borehole of uniform radius $r = a$, and a rectilinear drillstring assumed to initially lie along the bottom generator of the cylindrical borehole surface (see the left sketch in Figure 2); the location of various points along the drillstring is identified by the arclength coordinate $0 \le s \le S_0$ measured from O, with S_0 being the total drillstring length. The inclination of the borehole relative to the vertical axis (OX_3) is controlled by the angle $\beta \in [0°, 90°]$. The drillstring is assumed to be axially fixed at the lower end ($s = S_0$) and free to move at the other end ($s = 0$), while being loaded by distributed gravitational forces acting in the vertical plane (i.e., in the direction of OX_3); there are also distributed (Coulomb) frictional forces characterised by the frictional coefficient $\eta \in (0, 1)$. It is further assumed that the drillstring remains in full contact with the borehole along its entire length (at least) until buckling takes place. As shown

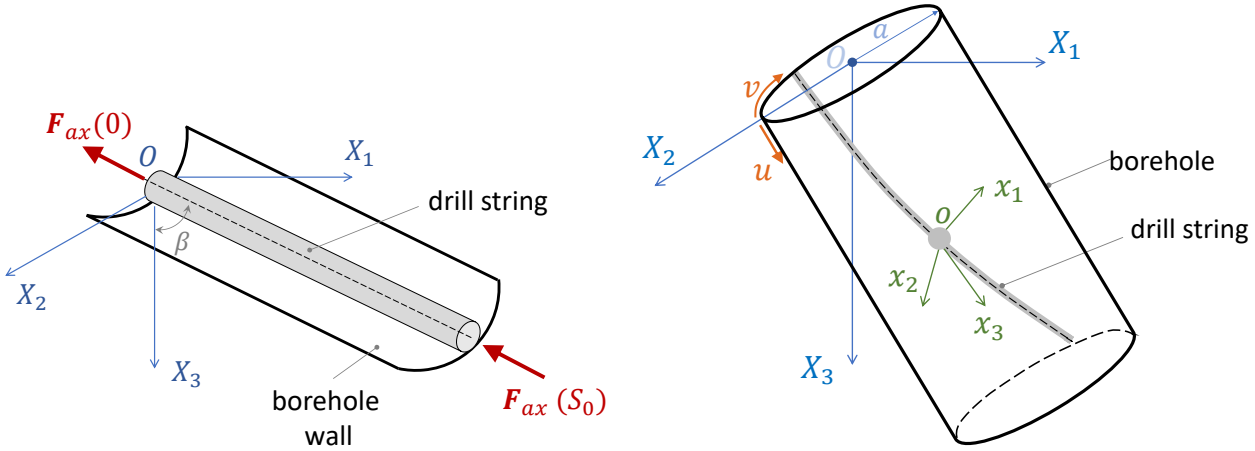

Figure 2: The DS configuration studied in [29] and [36].

in [29], the inhomogeneous axial force along the axis of the drillstring is given by

$$F_{ax}(s) = f_g(\cos\beta - \eta\sin\beta)(S_0 - s) - R\,, \qquad (R \equiv -F_{ax}(S_0))\,; \tag{2.1}$$

the notation f_g used here stands for

$$f_g := g(\rho_{st} - \rho_\ell)e\,,$$

where ρ_{st} and ρ_ℓ represent the densities of the drillstring material and the drilling fluid, respectively, while e denotes the cross-sectional area of the cylindrical drillstring pipe. Both [29] and [36] contain some confusing information about R; in the former reference this is incorrectly identified as $F_{ax}(0)$ (page 428), while in the latter it is stated (page 29) that $F_{ax}(0) = f_g(\cos\beta - \eta\sin\beta)S_0$ – if taken at face value, this statement in conjunction with equations (19) and (21) in the same reference would render $R \equiv 0$.

To describe the buckled configuration of the drillstring (see the right sketch in Figure 2), use is made of a parametrisation (u, v) of the cylindrical borehole, with the parameter u being directed along the cylinder generator, while v identifies the (angular) position of a point on a transverse cross-section (which is a circle of radius 'a'). Thus, the deformed axis of the drillstring is uniquely characterised by $(u(s), v(s))$, $0 \le s \le S_0$. Using the method of adjacent equilibrium, Gulyayev *et al.* [29] showed that the buckling equation for the above situation can be reduced to a single fourth-order differential equation in $y(s) := a\delta v(s)$, where δv is an infinitesimal increment of $v \equiv v(s)$. More precisely,

$$y'''' + \left[-\frac{f_g(\cos\beta - \eta\sin\beta)}{EI}(S_0 - s) + \frac{R}{EI} \right] y'' + \frac{f_g(\cos\beta - \eta\sin\beta)}{EI} y' + \frac{f_g \sin\beta}{aEI} y = 0\,, \tag{2.2}$$

where the 'dash' indicates differentiation with respect to the arclength variable 's', E is the Young's modulus for the drillstring, and I denotes the second moment of area of its annular transverse cross-section. This equation can be cast in a more convenient form by introducing the following non-dimensional quantities

$$\Gamma := \frac{f_g S_0^3}{EI}\,, \qquad \mu := \frac{S_0}{a}\,, \qquad \lambda := \frac{RS_0^2}{EI}\,, \qquad \rho := \frac{s}{S_0}\,, \tag{2.3}$$

so that (2.2) becomes

$$\frac{d^4y}{d\rho^4} + \big[-\Gamma(\cos\beta - \eta\sin\beta)(1-\rho) + \lambda \big] \frac{d^2y}{d\rho^2} + \Gamma(\cos\beta - \eta\sin\beta)\frac{dy}{d\rho} + \mu\big(\Gamma\sin\beta\big) y = 0\,; \tag{2.4}$$

note that the range of the original independent variable $0 \le s \le S_0$ has changed to $0 \le \rho \le 1$.

Equation (2.4) is not suitable for an asymptotic analysis as the order of magnitude of the quantities defined in (2.3) is not yet known. With this in mind, we now turn to considering the numerical values used in [29, 36] to settle this issue; the outer and inner diameters of the DS pipe are denoted by d_1 and d_2, respectively. In the references just cited $E = 2.1 \times 10^{11}$ Pa, $\rho_{st} = 7.8 \times 10^3$ Kg/m^3, $\rho_\ell = 1.3 \times 10^3$ Kg/m^3, $d_1 = 0.2$ m, $d_2 = 0.18$ m, $e = \pi(d_1^2 - d_2^2)/4 \simeq 5.97 \times 10^{-3}$ m^2, $I = (\pi/64)(d_1^4 - d_2^4) \simeq 2.7 \times 10^{-5}$ m^4, $\eta = 0.2$, $a = 0.166$ m, while S_0 was either 500.0 m or 1000.0 m. Assuming the smaller value for the length of the drillstring, the formulae (2.3) yield $\mu \simeq 3.01 \times 10^3$ and $\Gamma \simeq 8.39 \times 10^3$; for $S_0 \simeq 1000.0$ m the corresponding values are $\mu \simeq 6.02 \times 10^3$ and $\Gamma \simeq 6.70 \times 10^4$. These results suggest that $\mu \gg 1$ and a possible regime of interest for equation (2.4) would correspond to $\Gamma = \mathcal{O}(\mu)$, so we write

$$\Gamma = \Gamma_0 \mu\,, \qquad \Gamma_0 = \mathcal{O}(1)\,. \tag{2.5}$$

The use of this assumption in (2.4) leads to the alternative form

$$\frac{d^4y}{d\rho^4} + [-\mu\mathcal{A}(1-\rho) + \lambda] \frac{d^2y}{d\rho^2} + \mu\mathcal{A}\frac{dy}{d\rho} + \mu^2\mathcal{B}y = 0\,, \tag{2.6}$$

where

$$\mathcal{A} \equiv \mathcal{A}(\eta, \beta) := \Gamma_0(\cos\beta - \eta\sin\beta)\,, \qquad \mathcal{B} \equiv \mathcal{B}(\eta, \beta) := \Gamma_0 \sin\beta\,. \tag{2.7}$$

It is typically assumed that the ends of the drillstring are simply supported, which requires the usual boundary conditions

$$y = \frac{d^2y}{d\rho^2} = 0\,, \qquad \text{for } \rho = 0, 1\,. \tag{2.8}$$

The fourth-order differential equation (2.6) subject to the constraints (2.8) constitutes a boundary-value problem in which λ plays the role of an eigenvalue. The presence of the variable coefficients

makes it impossible to solve this analytically (except in special cases) but we can take advantage of the presence of the asymptotic parameter $\mu \gg 1$ to find suitable approximations for its solutions. We remark in passing that the aforementioned boundary eigenvalue problem resembles closely that studied recently in connection with the self-buckling of an equatorial spherical shell segment [31].

Before examining the asymptotic structure of (2.6)-(2.8) some observations are in order. Owing to the presence of the two parameters η (friction coefficient) and β (borehole inclination angle), the sizes of $\mathcal{A}$ and $\mathcal{B}$ are not *a priori* pre-determined; we shall assume that these quantities are $\mathcal{O}(1)$. For the latter quantity this means that β is not close to zero – indeed, this is the situation considered in [29, 36]. However, $\mathcal{A}$ may become equal to zero for $\beta = \beta_*$, with $\beta_* \equiv \cot^{-1}(\eta)$. As the coefficient of friction is typically between 0 and 1, the special value β_* will be between 90° and 45°. We will therefore assume that if η is given, the angles β considered are restricted by the requirement that $|\beta - \beta_*| = \mathcal{O}(1)$ (the angles being expressed in radians). As noted in previous investigations (e.g., [29, 36]), for $\beta = \beta_*$ equation (2.6) has constant coefficients (since $\mathcal{A} \equiv 0$) and hence the expression of the lowest eigenvalue can be obtained analytically since the buckling modes have a regular number of identical ripples. This is readily found by considering the trial function $y(\rho) = C\mathrm{e}^{\mathrm{i}\pi m\rho}$ (m, $C \in \mathbb{R}$, $\mathrm{i} \equiv \sqrt{-1}$) – note that its imaginary part satisfies the end constraints (2.8). On substituting this ansatz into (2.6), one finds λ as a function of the mode number $m > 0$. Further minimisation with respect to this latter quantity then produces the critical buckling values

$$\lambda_c^* = 2\mu\big(\Gamma_0 \sin\beta\big)^{1/2} \qquad \text{and} \qquad m_c^* = \mu^{1/2}\pi^{-1}\big(\Gamma_0 \sin\beta\big)^{1/4}. \tag{2.9}$$

Unfortunately, this simple result is only valid for $\beta = \beta_*$. When $\beta \simeq \beta_*$, the value λ_c recorded in (2.9) is still a good approximation for the buckling threshold because the corresponding true eigenmode resembles a sinusoidal regular pattern (although, strictly speaking, it is a globally modulated function – see Table 7-1, page 431 in [29]). For β-values "far" from β_*, and less than this special value, the eigenmodes are localised near the lower end of the string and one has to resort to a more in-depth analysis of the differential equation (2.6). We are going to unravel the corresponding asymptotic structure in §4 by taking advantage of the large parameter μ introduced in (2.3). In preparation for that, we will first explore briefly the numerical solutions of the boundary-value problem (2.6)-(2.8).

3 Numerical results

Examples of direct numerical simulations of the dimensional version of the linear bifurcation problem outlined in the previous section were presented in references [29] and [36]. Unfortunately, some of those results are incorrect as the eigenmodes shown there for $\beta > \beta_*$ do not correspond to the lowest positive eigenvalue of the corresponding buckling problem. With this in mind, we include below a quick discussion that clarifies the role played by the friction coefficient η and the inclination angle $0 < \beta \leq 90°$ on the solutions of (2.6)-(2.8). All the numerical results included in this section were obtained by using a spectral method [38, 39, 40], with an additional check being carried out with the help of the compound matrix method (e.g., see [41, 42]). The values of the various parameters appearing in equation (2.6) are those already mentioned in §2 (in the interest of brevity, only the value $S_0 = 500.0$ will be considered below).

The qualitative behaviour of the eigenmodes can be conveniently anticipated by expressing the inhomogeneous axial force (2.1) in non-dimensional form

$$\frac{F_{ax}S_0^2}{EI} = -\rho\mu\mathcal{A} + (\mu\mathcal{A} - \lambda)\,, \tag{3.1}$$

which represents essentially a straight line in 'ρ'. If $0 < \beta < \beta_*$ the gradient of this line is negative, so the maximum compression experienced by the drillstring will be near its right end ($\rho = 1$); for $\beta = \beta_*$ the axial force is constant for the entire range $0 \leq \rho \leq 1$ – this is the case corresponding to the regular buckling pattern already mentioned at the end of §2. Finally, for $\beta_* < \beta \leq 90°$ the gradient of the line (3.1) is positive, and the left end ($\rho = 0$) of the drillstring will be compressed the most. As a matter of fact, it turns out that if $\beta \neq \beta_*$, then the critical eigenmodes are either globally modulated or localised shapes, with the former situation occuring when $|\beta - \beta_*| \ll 1$.

The observations made above are supported by the numerical evidence included in Figures 3 and 4. In the interest of brevity we only show a small sample of eigenmodes obtained for $\eta = 0.2$ and a limited range of angles β, but these results are representative for other values as well. For reasons that will become apparent later on, in §4, we also include in the aforementioned figures the eigenmodes associated with the second lowest eigenvalue of the buckling problem (2.6)-(2.8).

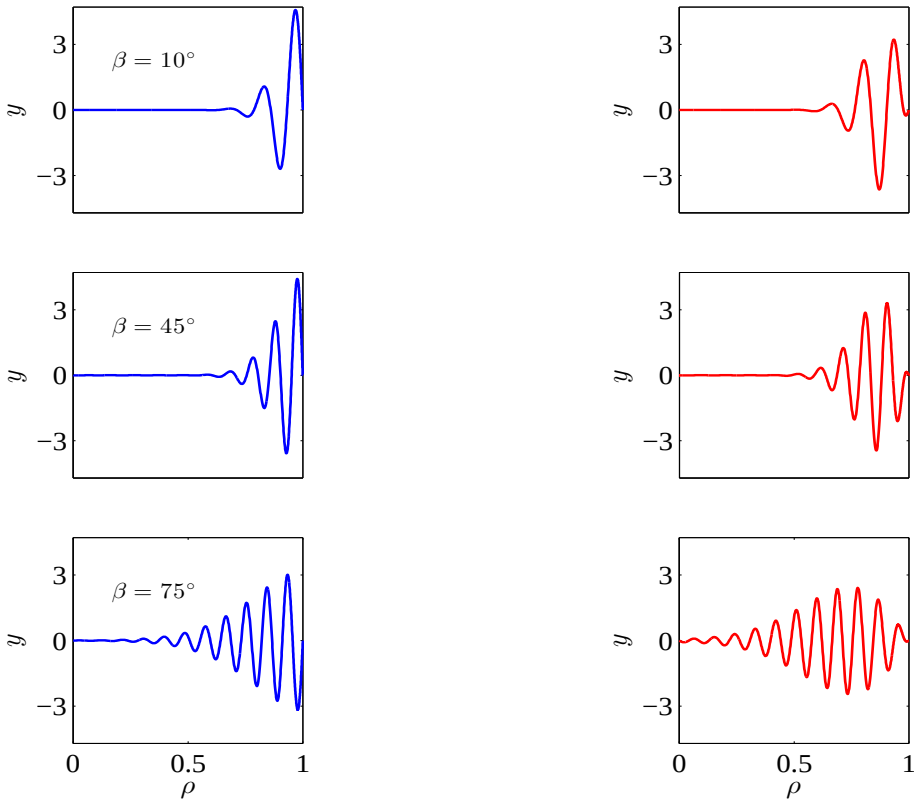

Figure 3: Samples of eigenmodes for the lateral buckling problem consisting of (2.6) subject to (2.8). The *critical* eigenmodes (in blue) appear in the left column, while those associated with the second smallest eigenvalue are shown next to them (in red); here, $\eta = 0.2$ and the borehole inclination angle $\beta < \beta_* \simeq 78.69°$ is shown individually for each of the three values considered.

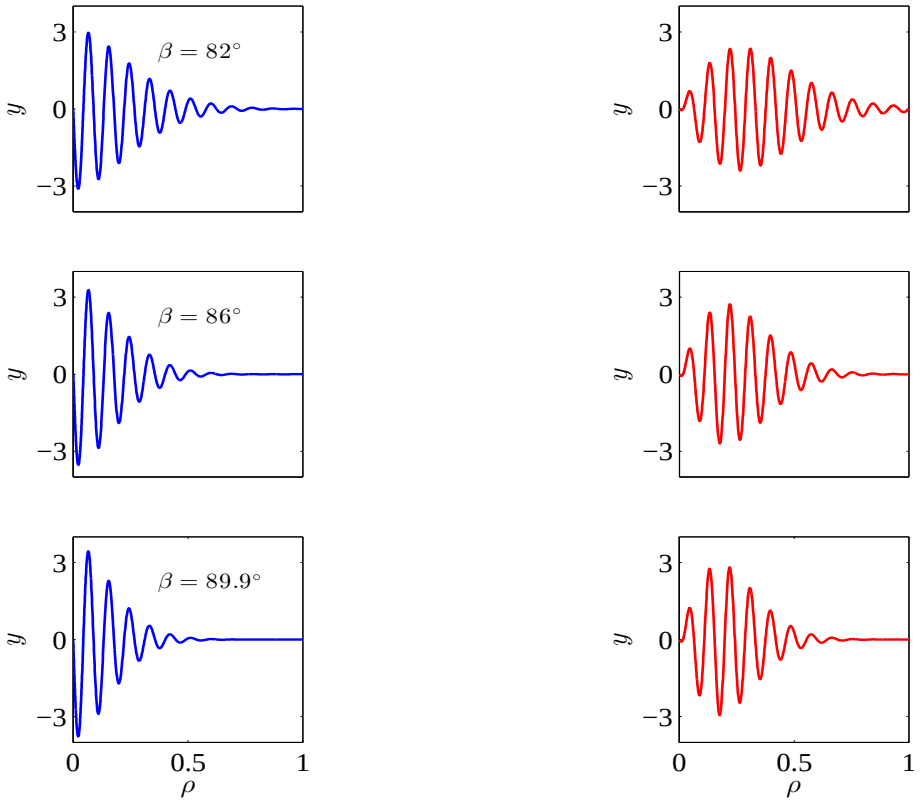

Figure 4: Same as per Fig. 3, except that here we consider values $\beta > \beta_* \simeq 78.69°$.

The critical modes illustrated in Figure 4 are different from those reported in [29] (see rows 5 and 6 in Table 7-1 on page 431) or in [36] (see Table 1, page 33). Those authors seem to have ended up with non-localised modes associated with higher points in the spectrum of the buckling problem. This is clearly the case as their predictions for the critical load λ_c when $\beta > \beta_*$ are larger than the values corresponding to the case $\beta < \beta_*$. To shed further light on this last statement, we summarise in Figure 5 the dependence $\lambda_c \equiv \lambda_c(\beta;\eta)$ for $30° \leq \beta \leq 90°$ and several values of the friction coefficient η (including $\eta = 0$, i.e. a frictionless drillstring). The information in the figure just mentioned suggests that the angle $\beta_* \equiv \cot^{-1}(\eta)$ marks the boundary between two distinct types of behaviour; in particular, as $\beta > \beta_*$ the critical load drops, which is in contrast to what references [29, 36] claimed.

It is somewhat easier to interpret the dependence of the critical load on the inclination angle β by shifting our attention to how the *critical* non-dimensional axial load at $\rho = 0$ varies in terms of the same angle. To this end, if $F_c(0)$ denotes this former quantity, we remark that (3.1) gives

$$F_c(0) \equiv \frac{F_{ax}^c(0)S_0^2}{EI} = \mu\mathcal{A} - \lambda_c\,, \tag{3.2}$$

where F_{ax}^c is the critical axial force obtained from (2.1) by letting $\lambda \to \lambda_c$ (see also the definition of λ in (2.3)).

Samples of plots for $F_c(0)$ versus β are recorded in Figure 6 for the same values of the friction coefficient as in the previous figure; identical colour-coding is used for the corresponding curves. Several noteworthy features that transpire from these plots are mentioned briefly next. For example, $F_c(0)$ turns out to be compressive for all values of β and η considered, irrespective of the location where the

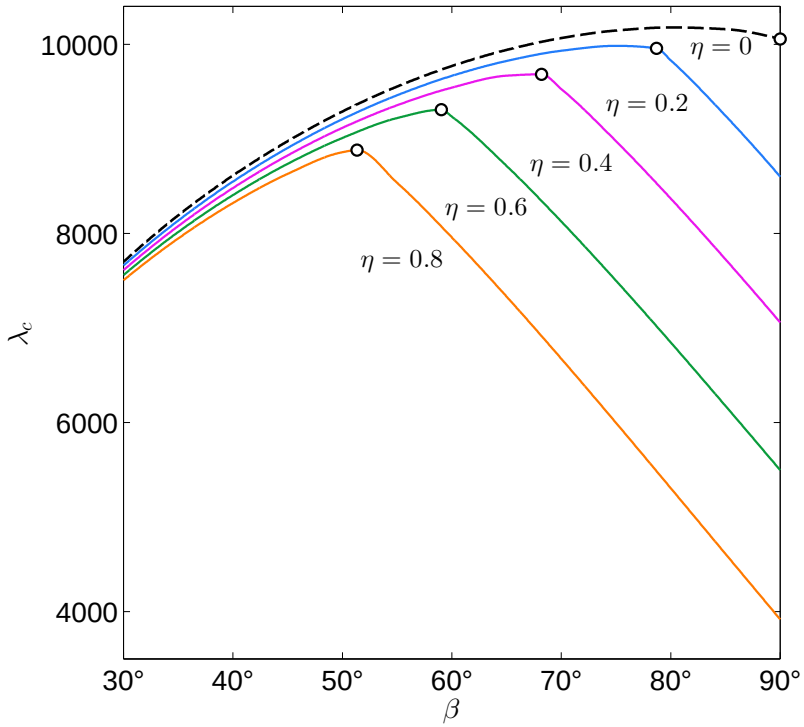

Figure 5: The dependence of the critical load λ_c on the borehole inclination angle $30° \leq \beta \leq 90°$ for different values of the friction coefficient $\eta \in \{0, 0.2, 0.4, 0.6, 0.8\}$; a vertical borehole has $\beta = 0°$, while for a horizontal one $\beta = 90°$. The white circular marker on each of the above curves corresponds to the point (β_*, λ_c^*) associated with the periodic deformation pattern mentioned at the end of §2.

buckling deformation is localised. For μ-values larger than the one considered in this section, $F_c(0)$ might end up being tensile [36] (see first row of the table on page 35 in that reference). It is also clear that the absolute value of the critical axial force at the left end of the DS increases with β. This is unsurprising since for a steep borehole the weight of the DS contributes more to the compression experienced by its lower end. On the other hand, in an almost horizontal borehole the compressive forces provided at the left end of the DS must be slightly larger in order for buckling to occur; this corresponds to the lower parts of the curves extending to the right of the white markers seen in Figure 6. The deformations associated with points on those curve segments are localised near the left end of the DS; this is rather unexpected and might be attributed to the rather crude modelling of the frictional forces in the model proposed by Gulyayev *et al.* [29, 36]. Finally, we should note that $F_c(0)$ is rather insensitive to the frictional forces for $\beta > \beta_*$, whereas for $\beta < \beta_*$ the opposite is true.

The numerical findings described in this short section are in agreement with the qualitative observations made vis-à-vis the non-dimensional axial force (3.1). However, there is an important caveat regarding the differential equation (2.6). Our study (as well as the work in [29, 36]) is based on the *a priori* assumption that the equation remains valid at all "times" during the loading phase and the incipient buckling of the drillstring. This assumption is needed because (2.1) incorporates the effect of frictional forces, which in turn require continuous contact between the drillstring and the borehole. When the borehole is horizontal, or close to horizontal (i.e., $\beta \simeq 90°$), this assumption may not be true; furthermore, in a practical drilling scenario there will be imperfections – either structural or

related to how the load is being applied relative to the axis of the drillstring. As a consequence, the deformation experienced by our configuration might not take place as hypothesised in the model studied in this paper. This shortcoming is shared to a large degree by all previous attempts to deal with frictional forces in similar contexts (e.g., see [6] and the references therein).

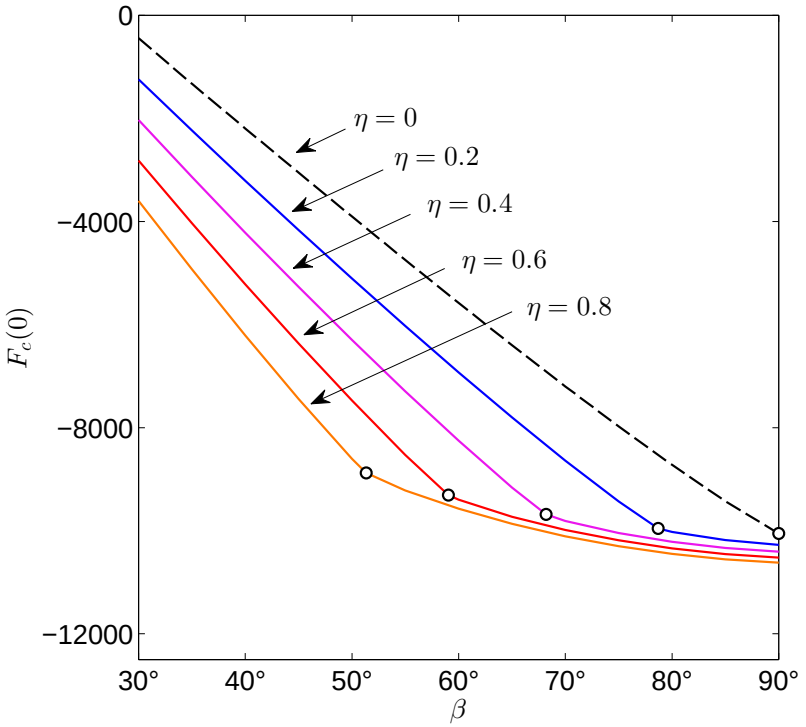

Figure 6: Another interpretation of Fig. 5 obtained by plotting (3.2) as a function of the inclination angle β. The white circular markers superimposed on the curves seen here have the same connotation as in the previous figure.

4 Asymptotic approximations

In the previous section we have seen that when the aspect ratio $\mu \gg 1$, the first two critical modes of the drillstring bifurcation problem adopt a localised structure provided that the borehole inclination angle β is not too close to the critical value $\beta_* \equiv \cot^{-1}(\eta)$. We shall designate these cases as $\beta \ll \beta_*$ and $\beta \gg \beta_*$, respectively (although, strictly speaking, this is an abuse of notation). We note that the solution samples in Figures 3 and 4 resemble closely some of those encountered in our previous studies [31, 32, 33, 35], an observation which suggests that the asymptotic strategy developed therein might be relevant to the boundary-value (2.6)-(2.8) as well. This is confirmed next.

4.1 The case $\beta \ll \beta_*$

According to §3, this regime corresponds to eigenmodes that are localised near $\rho = 1$, with the corresponding solutions displaying a multi-scale structure in which a fast spatial oscillation is modulated over a relatively narrow region adjacent to the lower end of the drillstring. Additional numerical work (see Table 7-2 on page 433 of [29]) suggests that the localisation process intensifies as $\mu \to +\infty$.

Standard scaling arguments can help establish the relevant orders of magnitude of the key terms in (2.6). Motivated by these considerations we introduce the re-scaled variable $Y > 0$ defined by

$$\rho = 1 - \mu^{-1/3} Y \,, \qquad \text{with} \qquad Y = \mathcal{O}(1) \,. \tag{4.1}$$

We will look for solutions of (2.6) satisfying an ansatz of the form

$$y = V(Y) \exp\left(\mathrm{i}\Omega \mu^{1/6} Y\right) , \qquad (\mathrm{i} \equiv \sqrt{-1}) \,, \tag{4.2}$$

where

$$V(Y) = V_0(Y) + \mu^{-1/6} V_1(Y) + \mu^{-1/3} V_2(Y) + \dots \,, \tag{4.3a}$$

$$\lambda = \lambda_0 \mu + \lambda_1 \mu^{2/3} + \lambda_2 \mu^{1/2} + \lambda_3 \mu^{1/3} + \dots \,, \qquad (\lambda_j \in \mathbb{R} \,,\ j = 0, 1, 2, \dots) \,; \tag{4.3b}$$

the constant $\Omega \in \mathbb{R}$ is unknown at this stage but will be found as part of the solution (e.g., see [35, 37]). The complex exponential term in (4.2) accounts for the spatial oscillations of the eigenmodes seen in Figures 3 and 4 – these oscillations take place on a $\mathcal{O}(\mu^{-1/2})$ scale which is much shorter than that described by the re-scaled independent variable Y in (4.1). It should be clear that the aforementioned ansatz is equivalent to the application of the method of multiple scales (e.g., [43, 44, 45, 46, 47]); this would correspond to introducing the spatial scales $\xi_1 \equiv \mu^{1/3}(1-\rho)$ and $\xi_2 \equiv \mu^{1/2}(1-\rho)$, and then regarding the dependent variables as functions of both (i.e., $y \equiv y(\xi_1, \xi_2)$). Past experience shows that the final results remain the same, so we shall take advantage of the simplified approach outlined above.

The zeroth-order equation amounts to a simple algebraic relation

$$\Gamma_0 \sin\beta - \Omega^2 \lambda_0 + \Omega^4 = 0 \qquad \Longrightarrow \qquad \lambda_0 = \Omega^2 + \frac{\Gamma_0 \sin\beta}{\Omega^2} \,. \tag{4.4}$$

It is clear that $\lambda_0 \equiv \lambda_0(\Omega^2)$ and, as we are looking for the lowest $\lambda_0 > 0$, we must search for the critical value(s) of Ω^2 by enforcing the usual stationarity condition $\partial\lambda_0/\partial(\Omega^2) = 0$. This equation yields the value $\Omega = \Omega_* > 0$,

$$\Omega_* := \left(\Gamma_0 \sin\beta\right)^{1/4} \qquad \Longrightarrow \qquad \lambda_0^* := \lambda_0\Big|_{\Omega=\Omega_*} = 2(\Gamma_0 \sin\beta)^{1/2} \,. \tag{4.5}$$

The information that transpires at first-order consists of

$$2\mathrm{i}\Omega(\lambda_0 - 2\Omega^2) V_0' + (\Gamma_0 \sin\beta - \lambda_0 \Omega^2 + \Omega^4) V_1 = 0 \,,$$

where the 'dash' stands for differentiation with respect to Y, a convention that will be employed for the rest of this section. This equation is identically satisfied for the values of λ_0 and Ω found in (4.5).

The next non-trivial piece of information emerges at the second order, namely

$$\gamma_1 V_0'' + \gamma_2 V_0 + \gamma_3 V_2 + \gamma_4 V_1' = 0 \,, \tag{4.6}$$

where

$$\gamma_1 := \Omega^2(\mathcal{A}Y - \lambda_1) \,, \quad \gamma_2 := \lambda_0 - 6\Omega^2 \,, \quad \gamma_3 := \Gamma_0 \sin\beta - \lambda_0 \Omega^2 + \Omega^4 \,, \quad \gamma_4 := 2\mathrm{i}\Omega(\lambda_0 - 2\Omega^2) \,.$$

Note that $\gamma_3 = \gamma_4 = 0$ when $\Omega = \Omega_*$ and $\lambda_0 = \lambda_0^*$, so that (4.6) can be re-stated in the simplified form

$$V_0'' - \frac{1}{4}(\mathcal{A}Y - \lambda_1) V_0 = 0 \,. \tag{4.7}$$

Equation (4.7) is amenable to further simplifications by adopting a suitable re-scaling of the independent variable

$$Z \equiv Z(Y) := 2^{-2/3}\mathcal{A}^{1/3}\left(Y - \frac{\lambda_1}{\mathcal{A}}\right), \tag{4.8}$$

whereupon it follows that $d^2\widehat{V}_0/dZ^2 - Z\widehat{V}_0 = 0$, with $\widehat{V}_0(Z) \equiv V_0(Y)$. The solution of interest is $\widehat{V}_0 = \mathrm{Ai}(Z)$, where 'Ai' is the usual Airy function that decays exponentially quickly as $Z \to +\infty$.

Given that our differential equation (2.6) has real-valued coefficients, both the real and imaginary parts of (4.2) represent approximations for two linearly independent solutions of (2.6), so the leading-order asymptotic solution we are looking for will be of the general form

$$y \simeq \left[C_1 \cos\left(\mu^{1/6}\Omega Y\right) + C_2 \sin\left(\mu^{1/6}\Omega Y\right)\right] \mathrm{Ai}(Z) + \ldots, \qquad (C_1,\, C_2 \in \mathbb{R}), \tag{4.9}$$

and it is this function that should be used in the boundary conditions $y = y'' = 0$ for $Y = 0$. The corresponding determinantal equation is

$$\mathrm{Ai}(Z)\mathrm{Ai}^{(1)}(Z) = 0 \qquad \text{for} \qquad Y = 0\,,$$

and we are then immediately led to

$$\lambda_1^* := \lambda_1\Big|_{\substack{\Omega_0=\Omega_0^* \\ \lambda_0=\lambda_0^*}} = \begin{cases} \zeta_0\,(2\mathcal{A})^{2/3}\,, & \text{if} \quad \mathrm{Ai}(Z(0)) = 0\,, \\ \\ \zeta_0'\,(2\mathcal{A})^{2/3}\,, & \text{if} \quad \mathrm{Ai}^{(1)}(Z(0)) = 0\,; \end{cases} \tag{4.10}$$

the superscript notation above was used to indicate differentiation with respect to Z, a convention that will be adopted tacitly henceforth. In this formula $(-\zeta_0) \simeq -2.338$ is the first zero of the Airy function 'Ai', while $(-\zeta_0') \simeq -1.0188$ represents the first zero of its derivative; that is, $\mathrm{Ai}(Z) = 0$ and $d\mathrm{Ai}/dZ = 0$ for $Z = -\zeta_0$ and $Z = -\zeta_0'$, respectively. Comparisons with direct numerical simulations of the boundary-value problem (2.6)-(2.8) indicate that it is the second expression in (4.10) which approximates the smallest eigenvalue when combined with (4.3b) and (4.5). Similarly, the other expression in (4.10) is associated with the second smallest eigenvalue of the original bifurcation equation. The leading-order approximation for the eigenmode corresponding to the latter is $y \simeq \mathrm{Ai}(Z(Y))\cos(\mu^{1/6}\Omega Y) + \ldots$, while the one for the former is $y \simeq \mathrm{Ai}(Z(Y))\sin(\mu^{1/6}\Omega Y) + \ldots$. It can be easily checked by direct calculations that these functions satisfy $y = y'' = 0$ when $Y = 0$, provided that λ_1 in (4.8) is chosen according to (4.10).

The two-term asymptotic approximation $\lambda_c \simeq \lambda_0^*\mu + \lambda_1^*\mu^{2/3}$, which follows immediately from (4.3b) together with (4.5) and (4.10), performs quite well but it represents an upper bound for the smallest and second smallest eigenvalues of the boundary-value problem (2.6)-(2.8). It is therefore of interest to explore the effect of the next few terms in the expansion of λ_c, and this is done next.

At the third-order, (2.6) throws an inhomogeneous Airy equation which can be cast in standard form by using the change of variable introduced in (4.8). Expressed in terms of that re-scaled variable the governing equation for V_1 can be shown to be

$$\frac{d^2\widehat{V}_1}{dZ^2} - Z\widehat{V}_1 = c_0\widehat{V}_0(Z) + c_1 Z\widehat{V}_0^{(1)}(Z) + c_2\widehat{V}_0^{(3)}(Z)\,, \tag{4.11}$$

with $\widehat{V}_1(Z) \equiv V_1(Y)$ and

$$c_0 := -(2\mathcal{A})^{-2/3}(\mathrm{i}\mathcal{A}\mathcal{B}^{-1/4} + \lambda_2)\,, \qquad c_1 := -\mathrm{i}(2\mathcal{A})^{1/3}\mathcal{B}^{-1/4}\,, \qquad c_2 := \frac{\mathrm{i}}{2}(2\mathcal{A})^{1/3}\mathcal{B}^{-1/4}\,.$$

A particular solution of (4.11) is given by

$$\widehat{V}_1 = \frac{1}{2}(2c_0 - c_1 + c_2)\widehat{V}_0^{(1)}(Z) + \frac{1}{4}(c_1 + c_2)Z^2\widehat{V}_0(Z) \equiv V_{1R}(Z) + \mathrm{i}V_{1I}(Z)\,, \tag{4.12}$$

with

$$V_{1R}(Z) := -(2\mathcal{A})^{-2/3}\lambda_2 \mathrm{Ai}^{(1)}(Z)\,, \qquad V_{1I}(Z) := \frac{1}{4}(2\mathcal{A})^{1/3}\mathcal{B}^{-1/4}\left[\mathrm{Ai}^{(1)}(Z) - \frac{1}{2}Z^2\mathrm{Ai}(Z)\right]. \tag{4.13}$$

Given the form of the ansatz (4.2), we get two potential contributions coming from the $\mathcal{O}(\mu^{-1/6})$-term in the asymptotic expansion (4.3a); these correspond to

$$\widetilde{y}_1(Y) := V_{1R}(Z)\cos(\mu^{1/6}\Omega Y) - V_{1I}(Z)\sin(\mu^{1/6}\Omega Y)\,, \tag{4.14a}$$

$$\widetilde{y}_2(Y) := V_{1R}(Z)\sin(\mu^{1/6}\Omega Y) + V_{1I}(Z)\cos(\mu^{1/6}\Omega Y)\,. \tag{4.14b}$$

Next, we examine the boundary conditions that need to be satisfied when $Y = 0$. This is best done by considering separately the two cases mentioned in (4.10).

If $\mathrm{Ai}^{(1)}(Z(0)) = 0$, we find $\widetilde{y}_1(Y=0) = V_{1R}(-\zeta_0') = 0$, while

$$\left.\frac{d^2\widetilde{y}_1}{dY^2}\right|_{Y=0} = -\mu^{1/3}\Omega^2 V_{1R}(-\zeta_0') - \mu^{1/6}\Omega(2\mathcal{A})^{1/3}V_{1I}^{(1)}(-\zeta_0') + \underline{(2\mathcal{A})^{2/3}V_{1R}^{(2)}(-\zeta_0')}\,.$$

The first two terms on the right-hand side of this equation are zero by default – see (4.13), whereas the underlined term is different from zero unless $\lambda_2 = 0$. Thus, the function $\widetilde{y}_1$ satisfies both boundary conditions at $Y = 0$ provided that λ_2 is chosen to be zero. With the benefit of hindsight, we note that the underlined term yields an $\mathcal{O}(\mu^{-1/6})$ contribution that can, in principle, be combined with a term of similar size that emerges in the boundary condition at next order, but this only gives a linear relationship between λ_2 and λ_3 (and thus both coefficients remain undetermined at that stage).

For the case $\mathrm{Ai}(Z(0)) = 0$ the situation is a bit more complicated. Trying to satisfy the boundary conditions at $Y = 0$ by using each of the two functions in (4.14), or a suitably constructed linear combination of both is not possible unless $\widehat{V}_1 \equiv 0$ and $\lambda_2 = 0$. Since the ansatz (4.3) needs a few amendments, the discussion of this case will be postponed until we complete the analysis for the critical buckling mode.

Information about λ_3 in (4.3b) emerges at the next order. For the case $\mathrm{Ai}^{(1)}(Z(0)) = 0$ we find another inhomogeneous Airy equation that can be re-scaled as before, and assumes the form

$$\frac{d^2\widehat{V}_2}{dZ^2} - Z\widehat{V}_2 = (d_1 + d_2Z^2)\widehat{V}_0(Z) + (d_3 + d_4Z^3)\widehat{V}_0^{(1)}(Z)\,, \tag{4.15}$$

with

$$d_1 := -(2\mathcal{A})^{-2/3}\lambda_3\,, \quad d_2 := \frac{1}{16}(2\mathcal{A})^{2/3}\mathcal{B}^{-1/2}\,, \quad d_3 := 2d_2\,, \quad d_4 := -d_2\,.$$

A particular solution of this equation is

$$\widehat{V}_2 = d_1\widehat{V}_0^{(1)}(Z) - d_2\left[4\widehat{V}_0^{(2)}(Z) - 2\widehat{V}_0^{(5)}(Z) + \frac{1}{8}\widehat{V}_0^{(8)}(Z)\right]. \tag{4.16}$$

The $\mathcal{O}(\mu^{-1/3})$ contribution of (4.2) corresponds to the function $\widehat{V}_2(Z(Y))\sin(\mu^{1/6}\Omega Y)$. This satisfies the boundary conditions at $Y = 0$ provided that $\widehat{V}_2^{(1)}\big|_{Z=-\zeta_0'} = 0$ or, in terms of (4.16),

$$-d_1\zeta_0' + \frac{1}{2}d_2 = 0 \quad \Longrightarrow \quad \lambda_3 = \lambda_3^* := -\frac{1}{32\zeta_0'}(2\mathcal{A})^{4/3}\mathcal{B}^{-1/2} < 0\,. \tag{4.17}$$

To summarise, we have obtained a three-term asymptotic approximation for the smallest positive eigenvalue of the buckling problem (2.6)-(2.8); combining the result just found together with (4.5) and (4.10), our final formula reads

$$\lambda_c^{(I)} = 2\mathcal{B}^{1/2}\mu + \zeta_0'(2\mathcal{A})^{2/3}\mu^{2/3} - \frac{1}{32\zeta_0'}(2\mathcal{A})^{4/3}\mathcal{B}^{-1/2}\mu^{1/3} + \dots , \tag{4.18}$$

where the notations for $\mathcal{A}$ and $\mathcal{B}$ were recorded in (2.7), and the superscript on the left-hand side of (4.18) is used to indicate that this is the lowest eigenvalue of the aforementioned boundary-value problem.

Returning now to the approximation for the second smallest eigenvalue, we start by noting that the original ansatz (4.3) must be replaced by

$$V(Y) = V_0(Y) + \mu^{-1/3}V_2(Y) + \dots , \tag{4.19a}$$

$$\lambda = \lambda_0\mu + \lambda_1\mu^{2/3} + \lambda_3\mu^{1/3} + \dots , \tag{4.19b}$$

and we emphasise that these expressions are only applicable to the case when $Z(0) = -\zeta_0$. Since we have eliminated $\widehat{V}_1$, the corresponding equation for $\widehat{V}_2$ adopts a slightly simpler form

$$\frac{d^2\widehat{V}_2}{dZ^2} - Z\widehat{V}_2 = (d_1 - 3d_2Z^2)\widehat{V}_0(Z) - 2d_2\widehat{V}_0^{(1)}(Z) , \tag{4.20}$$

with the particular solution

$$\widehat{V}_2 = d_1\widehat{V}_0^{(1)}(Z) + d_2\left[2\widehat{V}_0^{(2)}(Z) - \frac{3}{5}\widehat{V}_0^{(5)}(Z)\right] . \tag{4.21}$$

The $\mathcal{O}(\mu^{-1/3})$ contribution of (4.2) corresponds to the function $\widehat{V}_2(Z(Y))\cos(\mu^{1/6}\Omega Y)$. To satisfy the requisite boundary conditions at $Y = 0$ (at leading-order, at least) requires that $\widehat{V}_2\big|_{Z=-\zeta_0} = 0$; then, a simple use of (4.21) produces

$$d_1 - \frac{3\zeta_0^2}{5}d_2 = 0 \quad \Longrightarrow \quad \lambda_3 = \lambda_3^* := -\frac{3\zeta_0^2}{80}(2\mathcal{A})^{4/3}\mathcal{B}^{-1/2} < 0 . \tag{4.22}$$

We are finally in a position to state the full three-term asymptotic approximation for the second lowest eigenvalue, $\lambda_c^{(II)}$ (say), of the original buckling problem (2.6)-(2.8)

$$\lambda_c^{(II)} = 2\mathcal{B}^{1/2}\mu + \zeta_0(2\mathcal{A})^{2/3}\mu^{2/3} - \frac{3\zeta_0^2}{80}(2\mathcal{A})^{4/3}\mathcal{B}^{-1/2}\mu^{1/3} + \dots . \tag{4.23}$$

The analysis included in this section requires only minor modifications to deal with the localisation near the left end ($\rho = 0$) of the drillstring. The full details are omitted but the relevant differences are outlined in the next section.

4.2 The case $\beta_* \ll \beta \leq 90^\circ$

As suggested by the samples of eigenmodes included in Figure 3, when $\mu \gg 1$ the localisation of the drillstring persists even for $\beta \gg \beta_*$. This phenomenon is readily captured by introducing the new boundary-layer variable $X > 0$ defined according to

$$\rho = \mu^{-1/3}X , \qquad \text{with} \qquad X = \mathcal{O}(1) .$$

The ansatz (4.2) together with (4.3) remain valid in this case as well, where now Y must be replaced by X and the coefficients λ_j in (4.3b) will be denoted by $\widetilde{\lambda}_j$ ($j = 0, 1, 2, \dots$) for clarity purposes. The "dispersion" relation that links Ω to the leading-order term of λ changes to

$$\Gamma_0 \sin\beta - (\widetilde{\lambda}_0 - \mathcal{A})\Omega^2 + \Omega^4 = 0 \qquad \Longrightarrow \qquad \widetilde{\lambda}_0 = \mathcal{A} + \Omega^2 + \frac{\Gamma_0 \sin\beta}{\Omega^2}\,. \tag{4.24}$$

Comparison of this result with (4.4) confirms its close resemblance to the earlier expressions. Trivial calculations indicate that equation (4.24) yields exactly the same value $\Omega = \Omega_* > 0$ as in (4.5), and then (4.24) gives

$$\widetilde{\lambda}_0^* := \widetilde{\lambda}_0\Big|_{\Omega=\Omega_*} = \Gamma_0(\cos\beta - \eta\sin\beta) + 2(\Gamma_0 \sin\beta)^{1/2}\,. \tag{4.25}$$

The next-order equations are very similar to those already discussed in §4.1 – the final results can be immediately scooped up from (4.18) and (4.23) by changing $\lambda_0 \to \widetilde{\lambda}_0$ and making the substitution $\mathcal{A} \to |\mathcal{A}|$ in the remaining terms; the vertical bars used here represent the absolute value function. For the sake of convenience, we list below the corresponding asymptotic approximations for the first two lowest eigenvalues

$$\widetilde{\lambda}_c^{(I)} = (\mathcal{A} + 2\mathcal{B}^{1/2})\mu + \zeta_0'(2|\mathcal{A}|)^{2/3}\mu^{2/3} - \frac{1}{32\zeta_0'}(2|\mathcal{A}|)^{4/3}\mathcal{B}^{-1/2}\mu^{1/3} + \dots\,, \tag{4.26a}$$

$$\widetilde{\lambda}_c^{(II)} = (\mathcal{A} + 2\mathcal{B}^{1/2})\mu + \zeta_0(2|\mathcal{A}|)^{2/3}\mu^{2/3} - \frac{3\zeta_0^2}{80}(2|\mathcal{A}|)^{4/3}\mathcal{B}^{-1/2}\mu^{1/3} + \dots\,. \tag{4.26b}$$

In Figure 7 the predictions of the asymptotic formulae for the critical load – see (4.18) and (4.26a), are compared against direct numerical simulations of the full buckling problem. The analytical predictions are presented as dashed curves and the circular markers correspond to the computed values. The agreement here is excellent, with the relative errors involved in those comparisons being about $\mathcal{O}(10^{-5})$, or even higher. While we have focused on just one set of physical parameters (see §2), this degree of accuracy is maintained for other values (provided that $\mu \gg 1$).

5 Concluding remarks

This paper offers a new asymptotic treatment for the classical problem of (static) lateral buckling of a long drillstring that remains in contact with the wall of an inclined straight borehole. The weight of the drillstring as well as the frictional forces experienced by this configuration are both accounted for, with the mathematical model being formulated as a boundary eigenvalue value problem for an angular displacement [29, 36]. Our key results correspond to the non-dimensional three-term asymptotic formulae (4.18), (4.23), and (4.26), which capture the dependence of the first two lowest eigenvalues on all the relevant physical parameters. The mathematical investigations reported herein have also revealed some discrepancies in some of the numerical results reported previously in the literature in connection with the model considered in this paper. In particular, our theoretical results suggest that for inclination angles $\beta > \beta_* \equiv \cot^{-1}(\eta)$ (with η being the friction coefficient), the deformation of the drillstring tends to concentrate near its left end as $\beta \to 90^{\circ +}$; the (corrected) direct numerical simulations included in §3 have also confirmed this feature.

Our interest in the model explored in this work was partially stimulated by the recent publication [31] in which the self-buckling of a shallow spherical equatorial segment was reduced to an equation akin to (2.6). In that work we relied on the use of a simplified WKB analysis to deliver highly accurate approximations for the first two lowest eigenvalues of the corresponding bifurcation equation.

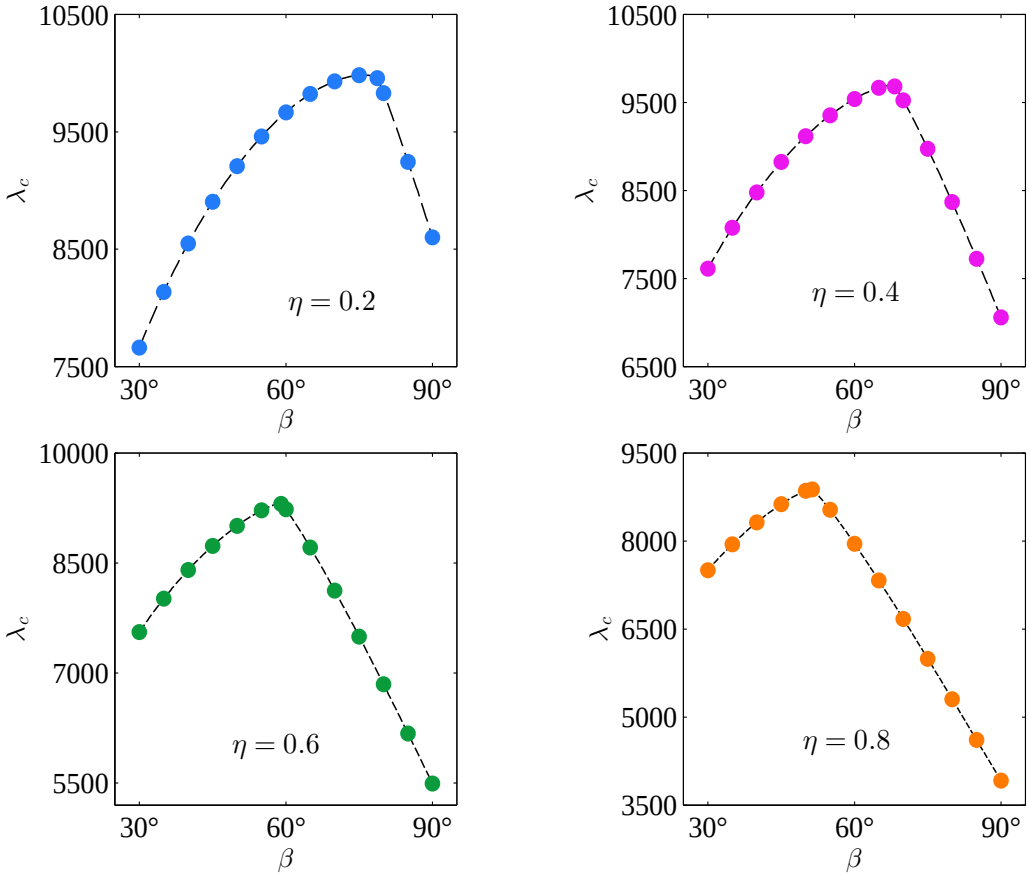

Figure 7: Comparisons of the asymptotic formulae (4.18) and (4.26a) with the direct numerical simulations recorded in Fig. 5. The dashed curves correspond to the theoretical predictions, while the circular markers represent the numerical data.

Although the boundary-layer approach was also tentatively pursued, the full details of the analysis were somewhat glossed over and the application of the boundary conditions for the asymptotic expansion was rather sketchy. In that sense, the present study fills in the missing steps and provides the basis for applying the asymptotic strategy discussed in §4 to similar linear boundary-value problems that exhibit localised oscillatory eigenmodes.

The main asymptotic ansatz (4.2) used in our analysis was phrased in terms of a complex exponential, but we have not followed through with the usual conventions associated with that notation (e.g., see [43, 44, 45]). For example, the expression stated in (4.9) is at odds with the spirit of the complex notation. If one insists on taking only the real part of the right-hand side of (4.2), then that would require introducing a phase angle θ_0 and replacing (4.2) with

$$y = \mathfrak{Re}\Big\{V(Y)\exp[\mathrm{i}(\Omega\mu^{1/6}Y - \theta_0)]\Big\}\,, \qquad \theta_0 \in \{0, \pi/2\}\,, \tag{5.1}$$

where $V(Y)$ is still as given in (4.3a), while $\mathfrak{Re}\{\dots\}$ denotes the real part of the quantity enclosed between the curly brackets. It is well known (e.g., [48, 49]) that such phase angles are not available from a purely theoretical linear analysis; they are typically identified from the numerical integration of the original boundary-value problem. The two values recorded in (5.1) were confirmed by comparing

the asymptotic approximations of the eigenmodes with the relevant direct numerical simulations of (2.6)-(2.8) which, in the interest of brevity, are not included here.

As mentioned in §1, the model studied in this paper is an extension of an earlier one proposed in [24]. By setting $\eta = 0$ in (2.6) we recover (more or less) the equation studied by Paslay and Bogy in the above work. Some minor discrepancies arise due to the fact that these authors left out the effect of the drilling fluid; also, the starting point for the derivation of their equations was nonlinear elasticity kinematics [25], whereas Gulyayev *et al.* [29] used the classical theory of rods [50, 51] (which ignores the Poisson effect). Dawson and Paslay [52] used the horizontal borehole results from [24] to come up with some sort of *empirical* formula for inclined boreholes. In light of this comment, it is instructive to re-interpret our non-dimensional result (4.18) in terms of the physical parameters. Simple algebraic manipulations indicate that

$$R_c = \underline{2\left(\frac{f_g EI \sin\beta}{a}\right)^{1/2}} + 1.6172 (f_g)^{2/3} (EI)^{1/3} (\cos\beta)^{2/3} - 0.0773\, a^{1/2} (f_g)^{5/6} (EI)^{1/6} (\cos\beta)^{4/3} (\sin\beta)^{-1/2} + \dots , \quad (5.2)$$

where R_c is the critical (buckling) value of R (the so-called 'weight-on-bit' or WOB for short). The formula proposed in [52] corresponds to the underlined term, but our result contains also some additional correction terms. Although the length of the DS has dropped out of (5.2), it should be kept in mind that the formula was derived under the assumption that $S_0 \gg a$. The authors of [52] remarked that the underlined term provides a reliable approximation for pipe lengths more than about 61 m (which corresponds to $\mu \gtrsim 367$).

Guided by the close analogy between the current study and the eigenvalue problem studied in [31], we have not been compelled to pursue here the effect of the borehole curvature. However, as shown numerically by Gulyayev *et al.* [29], the corresponding bifurcation equations for curved boreholes lead to a richer spectrum of localised eigenmodes. More specifically, the corresponding solutions are spatially focused at certain points along the length of the DS, and those locations must be identified as part of the solution. The multiple-scale asymptotic technique adopted in this paper can be extended to cope with such difficulties as past experience confirms (e.g., [53, 54]); the details of such an analysis have been recently completed in [55].

References

[1] Bourgoyne Jr., AT, Milheim, KK, Chenevert, ME, and Young Jr., FS. Applied Drilling Engineering. Richardson, TX: Society for Petroleum Engineering, 2014.

[2] Mitchell, RF, and Miska, SZ. Fundamentals of Drilling Engineering. Richardson, TX: Society for Petroleum Engineering, 2010.

[3] Belayneh, M. A review of Buckling in Oil Wells. Aachen: Shaker Verlag, 2006.

[4] Gao, D-L, and Huang, W-J. A review of down-hole tubular string buckling in well engineering. Pet Sci 2015; 12: 443–457.

[5] Mitchell, RF. Tubing buckling: the state of the art. SPE Drill Complet 2008; 23: 361–370.

[6] Cunha, JC. Buckling of tubulars inside wellbores: a review of recent theoretical and experimental works. SPE Drill Complet 2004; 19: 13–19.

[7] Timoshenko, SP, and Gere, JM. Theory of Elastic Stability (2nd ed.). New York, NY: McGraw-Hill Book Company, 1961.

[8] Brush, DO, and Almroth, BO. Buckling of Bars, Plates, and Shells. New York, NY: John Wiley & Sons, Inc., 1975.

[9] Leipholz, H. Stability of Elastic Systems. Alphen aan den Rijn, The Netherlands: Sijthoff & Noordhoff, 1980.

[10] Panovko, YG, and Gubanova, II. Stability and Oscillations of Elastic Systems. New York, NY: Consultants Bureau, 1965.

[11] Atanackovic, TM. Stability Theory of Elastic Rods. Singapore: World Scientific, 1997.

[12] Lubinski, A. A study of the buckling of rotary drilling strings. New York, NY: API Drilling and Production Practice, 1950.

[13] Lubinski, A. Influence of tension and compression on straightness and buckling of tubular goods in oil wells. In Proceedings of the 31st Annual Meeting of API, Production Bulletin **237**, 31–49 (1951)

[14] Lubinski, A, and Blenkarn, KA. Buckling of tubing in pumping wells, its effects and means for controlling it. AIME Pet Trans **210**, 73–88 (1957)

[15] Miska, SZ. Developments in Petroleum Engineering (vol. 1). Collected Works of Arthur Lubinski. Houston, TX: Gulf Publishing Company, 1987.

[16] Willers, FA. Das Knicken schwerer Gestänge. Z Angew Math Mech 1941; 21: 43–51.

[17] Greenhill, AG. Determination of the greatest height consistent with stability that a vertical pole or mast can be made, and of the greatest height to which a tree of given proportions can grow. Proc Camb Phil Soc 1881; 4: 65–73.

[18] Bernitsas, MM, and Kokkinis, T: Asymptotic behaviour of heavy column and riser stability boundaries. ASME J Appl Mech 1984; 51: 560–565.

[19] Rothman, M. The problem of an infinite plate under an inclined loading, with tables of the integrals of $\mathrm{Ai}(\pm x)$ and $\mathrm{Bi}(\pm x)$. Quart J Mech Appl Math 1954; 7: 1–7.

[20] Olver, FWJ, Lozier, DW, Boisvert, RF, and Clark, CW (Eds.). NIST Handbook of Mathematical Functions. Cambridge, UK: National Institute of Standards and Technology & Cambridge University Press, 2010.

[21] Dunayevsky, VA, and Judzis, A. Conservative and nonconservative buckling of drillpipe. SPE Annual Technical Conference and Exhibition, October 5-8, 1983, San Francisco, California. Paper Number SPE-11991-MS.

[22] Greenhill, AG. On the strength of shafting when exposed both to torsion and to end thrust. Proc Inst Mech Eng 1883; 34: 182–225.

[23] Pastrone, F. Torsional instabilities of Greenhill type in elastic rods. Rend Semin Mat Univ Padova 1992; 87: 77–91.

[24] Paslay, PR, and Bogy, DB. The stability of a circular rod laterally constrained to be in contact with an inclined circular cylinder. ASME J Appl Mech 1964; 31: 605–610.

[25] Green, AE, and Zerna, W. Theoretical Elasticity. Oxford, UK: Clarendon Press, 1960.

[26] Hetenyi, M. Beams on Elastic Foundation. Ann Arbor, MI: The University of Michigan Press, 1946.

[27] Selvadurai, AE. Elastic Analysis of Soil-Foundation Interaction. Amsterdam, The Netherlands: Elsevier, 1979.

[28] Bogy, DB, and Paslay, PR. Buckling of drill pipe in an inclined hole. ASME J Eng Ind 1964; 86: 214–218.

[29] Gulyayev, V, Glazunov, S, Glushakova, O, Vashchilina, E, Shevchuk, L, Shlyun, N, and Andrusenko, E. Modelling Emergency Situations in the Drilling of Deep Boreholes. Newcastle upon Tyne, UK: Cambridge Scholars Publishing, 2019.

[30] Lubinski, A, Althouse, WS, and Logan, JL. Helical buckling of tubing sealed in packers. J Pet Technol 1962; 14: 655–670.

[31] Coman, CD. Self-buckling of thin elastic shells: the case of a spherical equatorial segment. Z Angew Math Phys 2022; 73:228.

[32] Coman, CD, and Bassom, AP. Singular perturbations and torsional wrinkling in a truncated hemispherical thin elastic shell. J Elast 2022; 150: 197–220.

[33] Coman, CD, and Bassom, AP. Wrinkling of pre-stressed annular thin films under azimuthal shearing. Math Mech Solids 2008; 13: 513–531.

[34] Coman, CD, and Bassom, AP. On the wrinkling of a pres-stressed annular thin film in tension. J Mech Phys Solids 2007; 55: 1601–1617.

[35] Coman, CD, and Bassom, AP. Boundary layers and stress concentration in the circular shearing of thin films. Proc Roy Soc Lond A 2007; 463: 3037–3053.

[36] Musa, N, Gulyayev, V, Shlyun, N, and Aldabas, H. Critical buckling of drill strings in cylindrical cavities of inclined bore-holes. J Mech Eng Autom 2016; 6: 25–38.

[37] Coman, CD. Elastic instabilities caused by stress concentration. Int J Eng Sci 2008; 46: 877–890.

[38] Gardner, DR, Trogdon, SA, Douglas, RW. A modified tau spectral method that eliminates spurious eigenvalues. J Comp Phys 1989; 80: 137–167.

[39] Gheorghiu, CI. Spectral Methods for Non-Standard Eigenvalue Problems. New York, NY: Springer Nature B.V., 2014.

[40] Boyd, JP. Chebyshev and Fourier Spectral Methods (2nd ed.). Mineola, NY: Dover Publications Inc., 2000.

[41] Lindsay, K, and Rooney, CE. A note on compound matrices. J Comp Phys 1992; 133: 472–477.

[42] Ng, BS, and Reid, WH. A numerical method for linear two-point boundary-value problems using compound matrices. J Comp Phys 1979; 33: 75–85.

[43] Nayfeh, AH, and Mook, DT. Nonlinear Oscillations. New York, NY: John Wiley & Sons, Inc., 1979.

[44] Cheng, H. Advanced Analytic Methods in Applied Mathematics, Science, and Engineering. Boston, MA: LuBan Press, 2007.

[45] Kahn, PB. Mathematical Methods for Scientists & Engineers. New York, NY: John Wiley & Sons, 1990.

[46] Coman, CD. Asymptotic approximations for pure bending of thin cylindrical shells. Z Angew Math Phys 2017; 68: 82.

[47] Coman, CD. Localized elastic buckling: nonlinearities vs. inhomogeneities. IMA J Appl Math 2010; 75: 461–474.

[48] Tovstik, PE, and Smirnov, AL. Asymptotic Methods in the Buckling Theory of Elastic Shells. Singapore: World Scientific, 2001.

[49] Goldenweizer, AL, Lidskii, VB, and Tovstik, PE. Natural Oscillations of Thin Elastic Shells (in Russian). Moscow, URSS: Nauka, 1979.

[50] Svetlitsky, VA. Statics of Rods. Berlin, Germany: Springer, 2000.

[51] Love, AEH. A Treatise on the Mathematical Theory of Elasticity. Mineola, NY: Dover, 2003.

[52] Dawson, R, Paslay, PR. Drillpipe buckling in inclined holes. J Pet Technol 1984; 36: 1734–1738.

[53] Coman, CD. Oval cylindrical shells under asymmetric bending: a singular-perturbation solution. Z Angew Math Phys 2018; 69: 120.

[54] Coman, CD, and Bassom, AP. Wrinkling structures at the rim of an initially stretched circular thin plate subjected to transverse pressure. SIAM J Appl Math 2018; 78: 1009–1029.

[55] Coman, CD. On the localised buckling of drillstrings in curved boreholes. (Preprint, School of Computing and Engineering, University of Huddersfield, 2023).